Robust Direction-of-Arrival Estimation and Signal Separation Method for Integrated Sensing and Communication

Ming Chen, Liang Jin, Zheng Wan, Zheyuan Deng, Bo Zhang, Yajun Chen, and Kaizhi Huang

***Abstract*—In this study, we designed a single-channel direction-of-arrival (DOA) estimation and signal separation algorithm based on a grouping scheme for the time-varying metasurfaces (TVMs) for integrated sensing and communication systems. In this scheme, the harmonic effect of the TVM was used to transform the received single-channel signal into a multi-channel signal through an orthogonal Fourier coefficient matrix. After achieving multi-channel DOA estimation, the corresponding weighted beam pointing was designed for signal separation. By applying a periodic modulation function on the TVM to modulate the incident signal, the signal was mapped to a multi-dimensional received space to recover the multi-channel received signal. Thus, conventional multi-channel algorithms could be used on the single-channel signal for DOA estimation. Next, we designed a sub-surface weighted beam pointing to maximize the received signal signal-to-interference-plus-noise ratio. Simulation results revealed that the proposed scheme of DOA estimation can exhibit performances comparable to that of the conventional multi-channel antenna array. Moreover, the signal separation scheme designed based on this method was robust and could maintain good signal separation ability under a low signal-to-noise ratio.**

***Index Terms*—Blind source separation, direction of arrival (DOA) estimation, time-varying metasurface (TVM), weighted beam.**

I. Introduction

With the sixth generation (6G) mobile network emerging, ultra-large multiple-input multiple-output antenna arrays, millimeter wave, terahertz, and other technologies that can provide high-frequency bands, large bandwidth operation, and dense distribution will become increasingly prominent [1]. Extremely high throughput, reliability, and ultra-low latency are critical to achieve sense and control of the wireless communication environment required in 6G [2].

Integrated sensing and communication (ISAC) is a key technology of 6G mobile networks and has attracted considerable research attention. Unlike conventional communication systems, ISAC exhibits both sensing and communication attributes, avoiding wastage of wireless communication resources due to separate designs and achieving mutual benefits for both sides [3]. ISAC wireless communication systems should be improved using target positioning and channel sensing capabilities [4]. By integrating sensors and communication technologies, 6G mobile networks can achieve more efficient data transmission and smarter sensing capabilities, providing a superior service experience for various application scenarios.

In the ISAC system, the direction of arrival (DOA) are key parameters for achieving positioning and sensing functions, which can be used to assist terminal positioning, low-complexity beamforming, precise pilot and resource allocation, and effective interference suppression [5]. Many DOA estimation methods have been exploited in past research. The multi-signal classification (MUSIC) algorithm [6], signal parameter estimation through rotational invariance techniques (ESPRIT) algorithm [7], and related improved subspace-based algorithms have been used to provide high-precision DOA estimation results. Compressed sensing algorithms represented by orthogonal matching pursuit (OMP) [8] are attracting considerable research attention.

Meanwhile, the blind source separation (BSS) is a critical topic of research in signal processing and can be used to separate signal and interference signals to considerably improve the performance of wireless communication systems [9]. In BSS, the received signals are used without any prior information to recover the source signal [10]. Classic algorithms include the fast independent component analysis (FastICA) [11] and the joint approximative diagonalization of eigen matrix (JADE) algorithms [12]. In addition, nonnegative matrix factorization (NMF) algorithms are presented, such as the projective NMF [13] and the incremental NMF algorithm [14].

However, DOA estimation and BSS technology are based on multi-channel antenna arrays [15]. Multi-channel reception incorporates multiple radio frequency (RF) links, which require a complex hardware structure and high-power consumption. Using single-channel antenna arrays can solve the aforementioned problems. In the context of a single-channel antenna array, each constituent element is integrated with a unified RF chain, thereby endowing the system with the merits of

Manuscript received April 1, 2024; revised September 22, 2024; approved for publication by Zhu, Zhengyu Guest Editor, November 10, 2024.

This work was supported by the National Natural Science Foundation of China under Grant U22A2001, National University of Defense Technology 2021 Campus Project under Grant ZK21-43, National Social Science Fund Project under Grant SKJJ-x-067, Program of Song Shan Laboratory under Grant 221100211300-01 and the National Key Research and Development Program of China under Grant 2022YFB2902202.

M. Chen, L. Jin, Z. Deng, Y. Chen, and K. Huang are with the PLA Strategic Support Force Information Engineering University, Zhengzhou 450001, China, email: chenmingxd@126.com, liangjin@263.net, zy_deng_cc@outlook.com, chenyajun_cool@126.com, huangkaizhi@tsinghua.org.cn.

B. Zhang is with the School of International Relations, National University of Defense Technology, email: zb100403@123.com.

Z. Wan is with the Intelligent Gaming and Decision-making Laboratory, PLA Academy of Military Science, Beijing 100000, China, email: wanzheng18@alumni.hust.edu.cn.

L. Jin and Z. Wan are the corresponding authors.

Digital Object Identifier: 10.23919/JCN.2024.000068

1229-2370/24/$10.00 © 2024 KICS

streamlined architecture and minimized power expenditure. The signal processing within such an array demands the acquisition and subsequent manipulation of signals derived from a solitary observation channel, necessitating the exploitation of the intrinsic characteristics of the observed signal. This endeavor, which entails the isolation and processing of the signal from a single data stream, is inherently complex and poses a formidable challenge in the realm of signal processing [16].

However, single-channel DOA estimation schemes exhibit problems such as low accuracy, high computational complexity, or weak anti-interference ability. Furthermore, single-channel DOA estimation schemes are limited by the spatial resolution of the antenna array. In extreme single-channel BSS, solving a larger quantity using a smaller quantity is extremely challenging [17]. However, after several years of development, multi-channel technology is maturing. In current single-channel algorithms, the single-channel problem is first converted into a multi-channel problem and subsequently solved using multi-channel methods.

Metasurfaces have emerged as a novel material that can actively regulate the amplitude, phase, and polarization of electromagnetic waves [18]. Metasurfaces exhibit low cost, low power consumption, and simple hardware structure, which have been widely used in wireless communication scenarios [19]–[21]. The metasurface is composed of a large number of configurable low-power passive electromagnetic elements, each of which can be adjusted in real time to flexibly configure the wireless propagation environment [22]–[24].

A study [25] proposed the time dimension and suggested time-varying metasurfaces (TVMs) for designing metasurfaces to provide a new degree of freedom for electromagnetic wave regulation. The harmonic processing capability by time modulation provides novel opportunities for single-channel reception to be converted into multi-channel reception [26], [27]. In a study [28], a direction-finding method based on TVM was proposed. In this method, the relationship between harmonics and arrival angles was used for estimation. In another study [29], the MUSIC algorithm was applied to the metasurfaces to achieve one-dimensional direction-finding. A study [30] used the OMP algorithm in direction-finding based on programmable metasurfaces.

We proposed a single-channel DOA estimation and signal separation algorithm based on a grouping scheme for TVM implementation. Foe only one channel, the harmonic effect of TVM is utilized to integrate sensing functions and maximize the received signal SINR.The main contributions of this study are illustrated as follows

1) In this scheme, single-channel signals are decomposed using harmonics generated by time modulation functions, and multi-channel reception is restored using orthogonal time modulation function Fourier coefficient matrices. Conventional multi-channel DOA estimation algorithms are then used to obtain high-resolution estimation results, and corresponding directional weighted beams are designed for signal separation.
2) We use a complex exponential function as the time modulation function to achieve uncorrelated responses between sub-surfaces. Furthermore, we install the weighted beams of various sub-surface points in different directions to achieve orthogonal spatial receiving space to recover independent multi-channel signals.
3) Simulation results demonstrated the effectiveness of the proposed scheme, and the recovered multi-channel receiving signals are comparable to those obtained by the DOA estimation capability of conventional multi-channel antenna arrays. The proposed signal separation scheme is extremely robust and not affected by the SNR of the received signal.

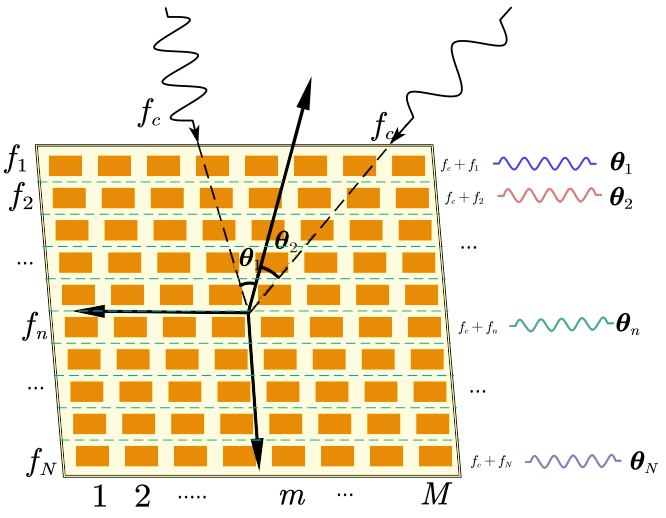

Fig. 1. Signal receiving model.

The organization of this article is as follows Section II introduces the signal reception model of time-modulated super-surfaces; Section III introduces the DOA estimation and signal separation scheme based on TVM; Section IV presents the simulation results of the proposed scheme; and finally, Section V concludes the article.

Notations: Lowercase and uppercase bold letters respectively represent vectors and matrices. For a matrix $\boldsymbol{Y}$, $\boldsymbol{Y}^{-1}$, $\boldsymbol{Y}^{T}$, and $\boldsymbol{Y}^{H}$ represent inversion, transpose, and Hermitian transpose. $\mathbb{C}^{M\times N}$ represents the space of a $N \times K$ complex matrix.

II. Signal Receiving Model

Referring to Fig. 1, consider a $N \times M$ column TVM with unit spacing of d. In this study, to achieve the separation of multiple signals with identical frequencies but distinct directions of arrival, we propose an approach that considers the signal separation associated with individual subsurfaces. Assuming each column unit is controlled by the different signal, each unit dynamically adjusts its reflectivity by applying a control voltage to a varactor diode. The TVM is illuminated by L narrow-band signals with the same frequency f, which originates from different directions in the z-axis incidence angle. The current work is dedicated to the development of

the signal separation strategy. As a result, the DoA estimation component has been intentionally simplified to facilitate the foundational exploration. Future endeavors will expand upon these preliminary findings, incorporating more sophisticated and multidimensional approaches to DoA estimation, thereby enhancing the methodological rigor and applicability of the proposed techniques. The received signal of the element in row N and column m can be expressed as follows

$$x_m(t) = \sum_{l=1}^{L} s_l(t) e^{j\beta(m-1)d\sin\theta_l} + n_m(t), \tag{1}$$

where s_l is the narrow-band signal from θ_l, $\beta = 2\pi/\lambda$ is the wave number with frequency f, and $n_m(t)$ is zero-mean Gaussian white noise with variance σ^2. For one-dimensional signals, the signals received by the same column between various sub-surfaces are consistent. Therefore, for a single-channel TVM, the received signal can be expressed as follows

$$y(t) = \sum_{n=1}^{N}\sum_{m=1}^{M} \Gamma_{mn}(t) x_m(t), \tag{2}$$

where $\Gamma_{mn}(t)$ is the time modulation function of the mth column of the nth sub-surface for which can be expressed as the linear combination of the harmonics

$$\Gamma_{mn}(t) = \sum_{k=-\infty}^{+\infty} c_{mnk} e^{j2k\pi f_n t}, \tag{3}$$

where f_n is the modulation frequency of each sub-surface and c_{mnk} serves as the kth harmonic's Fourier coefficient for $\Gamma_{mn}(t)$.

$$c_{mnk} = \frac{1}{T_n}\int_0^{T_n} \Gamma_{mn}(t) e^{-j2k\pi f_n t} dt, \tag{4}$$

where $T_n = 1/f_n$ is the modulation period of the nth sub-surface. For scenarios that demand low modulation rates but high precision, TVM dynamically controls the reflection coefficient of the component by applying a control voltage to the varactor diode. In contrast, for scenarios requiring high modulation rates, discrete TVMs are utilized to achieve the desired performance. This approach allows for the optimization of different modulation requirements while maintaining the efficiency and precision of the system. All elements are controlled by a modulation signal of the same frequency. Considering each sub-surface corresponds to one signal path, only one harmonic time modulation function is required, given by the following equation

$$\Gamma_{mn}(t) = b_{mn} e^{j\frac{2\pi}{T_n}t}, \tag{5}$$

where $b_{mn} = |b_{mn}| e^{j\phi_m}$ represents the complex coefficient of the modulation function. When the signal is projected on the complex plane, we can obtain a circle with an amplitude of $|b_{mn}|$, the phase continuously changes with an initial phase of ϕ_m, and T_n determines the speed of the phase change. Therefore, the received signal on the nth sub-surface can be expressed as follows

$$y_n(t) = \sum_{l=1}^{L}\sum_{m=1}^{M} b_{mn} e^{j\beta(m-1)d\sin\theta_l} s_l(t) e^{j2\pi f_n t} + n_n(t), \tag{6}$$

where $n_n(t) = \Gamma_{mn}(t) n_m(t)$ is the noise signal and the variance is σ^2.

Beacuse of the time modulation of the grouping TVM, the incident signal will be distributed over the modulation frequencies of each sub-surface. At the same time, different sub-surfaces will generate different patterns based on the complex coefficients of the modulation function to receive the signal. The nth sub-surface pattern can be expressed as

$$\varphi_n(\theta_l) = \sum_{m=1}^{M} b_{mn} e^{j\beta(m-1)d\sin\theta_l}. \tag{7}$$

III. Poposed DOA Estimation and Signal Separation Scheme

In this section, we propose a signal separation scheme based on TVM. In this scheme, we used various frequency time modulation functions and orthogonal patterns to receive signals to obtain a multi-dimensional signal receiving space for DOA estimation. Furthermore, we designed time modulation functions based on the estimation results to generate directional beams for signal separation. Therefore, this scheme can realize the integration of sensing and assistive communication using TVM.

A. DOA Estimation Scheme

According to the Nyquist theorem, when modulation frequency f_n is greater than or equal to the bandwidth of the signal $s_l(t)$, sidebands do not overlap, and each sideband signal and the center frequency signal can be separated using a filter. Therefore, we used time-modulated signals with various frequencies $(f_1, \cdots, f_N)$ between different sub-surfaces, and the direct spacing between each frequency was greater than the signal bandwidth to ensure that the signals did not overlap in the frequency spectrum. Therefore, in a single-channel receiver, the received signal passes through a low-noise amplifier, a mixer, a low-pass filter, and then an analog-to-digital converter to sample and obtain the received signal of each sub-surface, which can be expressed as follows

$$y_n(n) = \sum_{l=1}^{L} \varphi_n(\theta_l) s_l(n) + n_n(n), \tag{8}$$

where $s_l(n)$ is the baseband sampled signal of the narrowband signal $s_l(t)$, and $n_n(n) = b_{mn} n_m(n)$ is the noise signal. Therefore, considering N snapshots, the total received signal can be written as

$$\boldsymbol{Y}(n) = \boldsymbol{B}^T [\boldsymbol{A}(\theta)\boldsymbol{s}(n) + \boldsymbol{N}(n)], \tag{9}$$

where $\boldsymbol{Y}(n) = [y_1(n), \cdots, y_n(n), \cdots, y_N(n)]^T$ is the received signal for each sub-surface, $\boldsymbol{B} = \{b_{mn}\} \in \mathbb{C}^{M*N}$

is the complex coefficient matrix of the time modulation function, $\boldsymbol{A}(\theta) = [\boldsymbol{\alpha}(\theta_1), \cdots, \boldsymbol{\alpha}(\theta_l), \cdots, \boldsymbol{\alpha}(\theta_L)]$ represents the array flow pattern of the lth narrowband signal, $\boldsymbol{s}(n) = [s_1(n), \cdots, s_l(n), \cdots, s_L(n)]^T$ is the narrowband incident signal matrix, and $\boldsymbol{N}(n) = [n_1(n), \cdots, n_m(n), \cdots, n_M(n)]^T$ is the noise matrix. Here, the complex coefficient matrix is known. After sampling, the received signal matrix is reduced by left multiplying it with the inverse matrix to obtain the M-channel uniform linear array received signal matrix.

$$\begin{aligned}\bar{\boldsymbol{Y}}(n) &= \left(\boldsymbol{B}^T\right)^{-1}\boldsymbol{Y}(n) \\ &= \boldsymbol{A}(\theta)\boldsymbol{s}(n) + \boldsymbol{N}(n).\end{aligned} \tag{10}$$

To ensure the validity of the above conversion method, the complex coefficient matrix $\boldsymbol{B}$ should satisfy the row full rank condition. To ensure the best performance of the recovery and the feasibility of the scheme, we consider the weighted coefficient matrix in the beam scanning principle as the complex coefficient of the time modulation function, which can be expressed as

$$\boldsymbol{B} = \left[1, \cdots, e^{-j\beta m d\sin\theta}, \cdots, e^{-j\beta(M-1)d\sin\theta}\right]. \tag{11}$$

Beam scanning means that the main lobe of the directional diagram is shifted to θ, and the principle can be expressed as

$$\varphi(\theta) = \sum_{m=1}^{M} A e^{j\beta(m-1)d(\sin(\theta)-\sin(\theta_0))}. \tag{12}$$

Combining (7) and (12), we can obtain $b_{mn} = e^{-j\beta(m-1)d\sin\theta_n}$ by setting $\varphi(\theta) = \varphi_n(\theta)$. For various sub-surfaces, we selected different θ_n, so the time modulation function of the TVM in the mth column of the nth sub-surface can be expressed as follows

$$\Gamma_{nm}(t) = e^{j2\pi f_n(t-t_{nm})}, \tag{13}$$

where $t_{nm} = (m-1)T_n\sin\theta_n/2$ is the time-shift coefficient. Equation (1) reveals that when the sub-surface is based on the first column and each column is shifted by $T\sin\theta/2$, the phase difference caused by the incident angle θ can be canceled, so the peak direction of the directional pattern shifts by θ. In particular, for an M-column uniform array, each column can be shifted by T_n/M to obtain an orthogonal directional pattern, at which point the peak direction of each sub-surface coincides with the null of the remaining sub-surfaces, and patterns are shown in Fig. 2

The multi-channel received signal matrix is the foundation of all spatial spectrum estimation. Therefore, for ensuring the single-channel array model, we can use the time-modulated super-surface harmonic processing ability to recover the multi-channel received signal matrix and subsequently adopt all conventional DOA estimation methods. Here, we take the MUSIC algorithm as an example. The covariance matrix of the signal can be expressed as

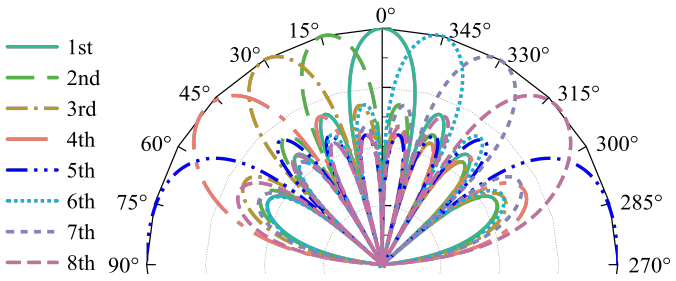

Fig. 2. Each sub-surface patterns.

$$\begin{aligned}\hat{R}_{YY} &= \frac{1}{N}\sum_{n=1}^{N} Y(n)Y^H(n) \\ &= A\hat{R}_{ss}A^H + \sigma^2 I,\end{aligned} \tag{14}$$

where $[\cdot]^H$ denotes the conjugate transpose operator, and

$$\hat{R}_{ss} = \frac{1}{N}\sum_{n=1}^{N} s(n)s^H(n). \tag{15}$$

Eigenvalue decomposition on $\hat{R}_{YY}$ can be expressed as

$$\begin{aligned}\hat{R}_{YY} &= U_s\Lambda_s U_s^H + U_N\Lambda_N U_N^H \\ &= \sum_{i=1}^{L}\lambda_i e_i e_i^H + \sum_{j=L+1}^{M}\lambda_j e_j e_j^H,\end{aligned} \tag{16}$$

where signal subspace U_s composed of eigenvector corresponding to the L larger eigenvalues of $\hat{R}_{YY}$, and noise subspace U_N composed of residual eigenvectors. As the signal and noise subspace are orthogonal, the virtual direction vector A^H is orthogonal to U_N, is described as

$$A^H U_N = 0. \tag{17}$$

As the impact of noise, (14) is only approximately 0. DOA estimates by searching for the optimal solution through spectral peaks, spectrum is given by

$$P(\theta) = \frac{1}{A^H(\theta)U_N U_N^H A(\theta)}. \tag{18}$$

B. Signal Separation Scheme

Based on the DOA estimation results $\hat{\theta} = \left[\hat{\theta}_1, \cdots, \hat{\theta}_l, \cdots, \hat{\theta}_L\right]^T$, we can optimize design of the time modulation function $\Gamma_{mn}(t)$, the diagram is depicted in Fig. 3.

For $N = L$, the number of sub-surfaces is the same as the number of signals, and each sub-surface completes the reception of one signal. We consider moving N signals to N different frequencies, and the received signal after sampling on the nth sub-surface can be expressed as follows

$$y_n(n) = \varphi_n(\theta_n)s_n(n) + \sum_{l\in L, l\neq n}\varphi_n(\theta_l)s_l(n) + n_n(n), \tag{19}$$

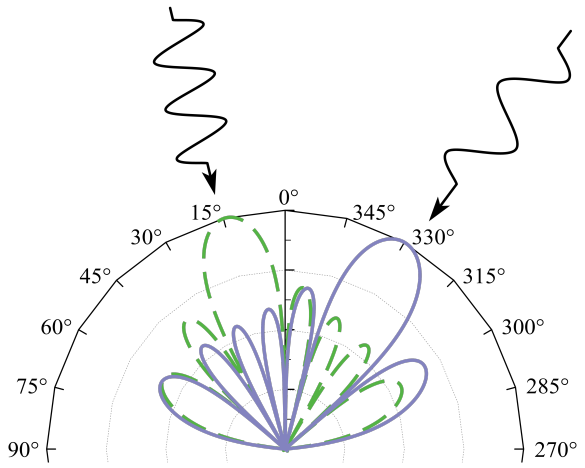

Fig. 3. Signal separation diagram.

The first term is the desired signal, the second term is the remaining signals considered interference signals, and the third term is the noise signal. In this study, the segregation of multi-path signals is accomplished by engineering directional radiation patterns on a per sub-surface basis that correspond to their respective propagation directions, culminating in each sub-surface retaining a single signal component. However, the resultant radiation patterns do not manifest complete orthogonality. Consequently, the efficacy of the separation is compromised when the incidence angle of interfering signals aligns with the high-gain regions proximal to the side lobes or the main lobe of the established patterns. The mean value of the signal-to-interference-plus-noise ratio (SINR) and correlation coefficient is considered after signal splitting to describe the signal separation effect. The ratio of the separated signal component to the residual signal component is referred to as the SINR. A higher SINR indicates a better ability to suppress interference and noise after separation, leading to improved separation performance, which can be expressed as follows

$$\begin{aligned}\eta &= \frac{1}{N}\sum_{n=1}^{N}\frac{\left|\varphi_n\left(\hat{\theta}_n\right)s_n\right|^2}{\sum_{l\in L,l\neq n}\left|\varphi_n\left(\hat{\theta}_l\right)s_l\right|^2+|n_n|^2} \\ &= \frac{1}{N}\sum_{n=1}^{N}\frac{P_S\left|B_nA\left(\hat{\theta}_n\right)\right|^2}{\sum_{l\in L,l\neq n}P_S\left|B_nA\left(\hat{\theta}_l\right)\right|^2+\sigma^2},\end{aligned} \tag{20}$$

where P_S is the signal transmission power, $B_n = \left[1,\cdots,e^{-j\beta(m-1)d\sin\phi_n},\cdots,e^{-j\beta Md\sin\phi_n}\right]$ is the weighting coefficient, and ϕ_n is the desired directional pattern of the nth sub-surface. In signal separation schemes, the design of the reflection coefficient primarily focuses on maximizing the received signal power while minimizing the power of interfering signals. In spatial filtering, this can be translated into maximizing the ratio of directional pattern gains corresponding to the arrival directions of the desired signal and the interfering signals. According to the measurement standard, the weighted beam generated by the sub-surface should have the largest gain difference in the direction of the incoming wave. Therefore, we can obtain the weighted directional pattern $\phi = [\phi_1,\cdots,\phi_n,\cdots,\phi_N]^T$, which can be expressed by

$$\begin{aligned}&\max_{\phi}\ \eta \\ &s.t.\phi\in\left[-\frac{\pi}{2},\frac{\pi}{2}\right].\end{aligned} \tag{21}$$

Therefore, the time modulation function can be expressed by

$$\begin{aligned}\Gamma_{nm}(t) &= e^{j2\pi f_n(t-t_{nm})}, \\ t_{nm} &= (m-1)\frac{T_n\sin\hat{\phi}_l}{2}\end{aligned} \tag{22}$$

The degree of similarity between the separated signal component and the original signal component is referred to as the correlation coefficient. A correlation coefficient closer to 1 indicates a higher degree of similarity between the two components, leading to better separation performance. The correlation coefficient between the source signal $s_l(n)$ and the separated signal $y_n(n)$ can be expressed as

$$\rho_{nl} = \rho(y_n, s_l) = \frac{\left|\sum_{i=1}^{N}y_n(i)\,s_l(i)\right|}{\sqrt{\sum_{i=1}^{N}y_n^2(i)\sum_{i=1}^{N}s_l^2(i)}}. \tag{23}$$

For $N > L$, we subdivide the sub-surfaces based on the signal energy ratio and use the additional sub-surfaces for signal shunting with a high energy ratio. This implies that multiple sub-surfaces will receive signals concurrently, and the weighted directional pattern will become $\phi = [\phi_1,\cdots,\phi_L,\phi_{N-L+1},\cdots,\phi_N]^T$

The single-channel DOA estimation and signal separation algorithm based on a grouping scheme can be optimized and summarized as Algorithm 1.

IV. Simulation Results

In this section, numerical simulation is used to evaluate the performance of DOA estimation methods and signal separation. After DOA estimation, signal separation was performed based on the estimation results, including DOA estimation accuracy and received SINR analysis. All statistical results are based on 100 Monte Carlo simulations.

Consider an 8×8 time-modulated super-surface, which is divided into eight sub-surfaces, each consisting of eight units with a unit spacing d of half a wavelength. The spatial filtering approach presented herein is predominantly contingent upon the precision of the DoA estimation outcomes, while the impact of diverse modulation techniques on signal separation is deemed to be inconsequential. Consequently, it is posited that the modulation format for the impinging narrowband signals shall be quadrature phase shift keying (QPSK) as a surrogate, the carrier frequency fc is 3.15 GHz and the bandwidth is 3 MHz. To simplify the analysis, only two narrow-band signals are considered. Therefore, the modulation frequency of each sub-surface is set as

Algorithm 1 Single-channel DOA estimation and signal separation algorithm

1. *Input* The receive signal x, the number of columns N of TVM, the number of array elements M, the wavelength λ, the distance between adjacent TVM elements d, time modulation function Γ, and Fourier coefficient B

2. Obtain the time modulated signal matrix $\boldsymbol{Y}(t) = \boldsymbol{\Gamma}^{\boldsymbol{T}} \boldsymbol{X}(t)$

3. Obtain the sampled and filtered signal matrix $\boldsymbol{Y}(n) = \boldsymbol{B}^T [\boldsymbol{A}(\theta)\boldsymbol{s}(n) + \boldsymbol{N}(n)]$

4. Obtain a multi-channel uniform linear array receiving signal matrix $\bar{\boldsymbol{Y}}(n) = \left(\boldsymbol{B}^T\right)^{-1} \boldsymbol{Y}(n)$

5. Estimating DOA using MUSIC algorithm $\hat{\theta} = \left[\hat{\theta}_1, \cdots, \hat{\theta}_l, \cdots, \hat{\theta}_L\right]^T$

6. Obtain weighted directional pattern $\phi = [\phi_1, \cdots, \phi_n, \cdots, \phi_N]^T$

7. *Output* Time-shift coefficient $t_{nm} = (m-1)\frac{T_n \sin\phi_n}{2}$

TABLE I
PARAMETERS FOR NUMERIC SIMULATION.

Symbol	Parameter	Value
M	Element number	8
d	Element spacing	$\lambda/2$
f_c	Carrier frequency	3.15 Ghz
f_s	Sampling frequency	5.76 Ghz
B	Bandwidth	3 Mhz

$(f_1 = \cdots = f_4 = -6\ Mhz, f_5 = \cdots = f_8 = 6\ Mhz)$ to ensure no aliasing between the received signals on each sub-surface. Therefore, the root mean square error (RMSE) of DOA estimation can be defined as follows

$$RMSE = \sqrt{\frac{1}{2J}\sum_{j=1}^{J}\sum_{l=1}^{2}\left(\hat{\theta}_l(j) - \theta_l\right)^2}, \tag{24}$$

where J is the number of Monte Carlo experiments 100, and $\hat{\theta}_l(j)$ is the jth Monte Carlo estimate of the lth signal. The relevant parameters are shown in Table I.

A. DOA Estimation Performance

In this section, we consider two co-channel signals with various arrival directions and obtain a multi-channel received signal matrix by processing the single-channel received signal using the scheme proposed in Section II. The DOA estimation performance is evaluated based on the received signal power spectrum, spatial spectrum, and estimated RMSE.

First, Fig. 4 displays the power spectrum of the received signal with incident directions $\pm 20°$ and $\pm 30°$. The black line represents the power spectrum of the original single-channel QPSK signal, and the red line represents the power spectrum of the signal recovered after time modulation. The figure reveals that because of the single-channel receiving of the original two-channel QPSK signal, only one power spectral line exists. After the time modulation of the super-surface, the original signal is modulated into different frequencies, and the response of various sub-surfaces to the incident signal differs considerably, which is jointly determined by the weighted array flow pattern corresponding to each sub-surface and the DOA of the incident signal. The final power spectrum map forms a new multi-dimensional data space for multi-channel received signal recovery.

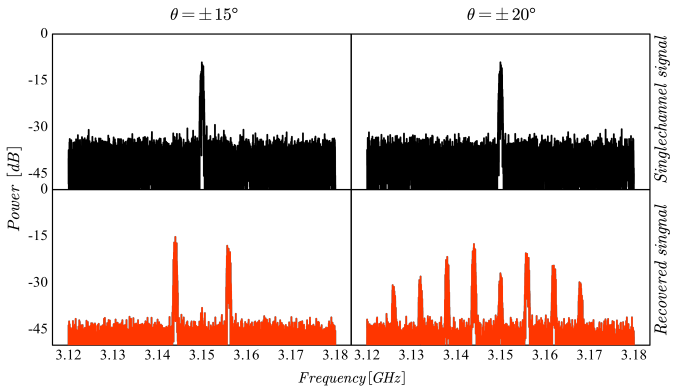

Fig. 4. Spectra distributions of the reflected signal with different incident angle.

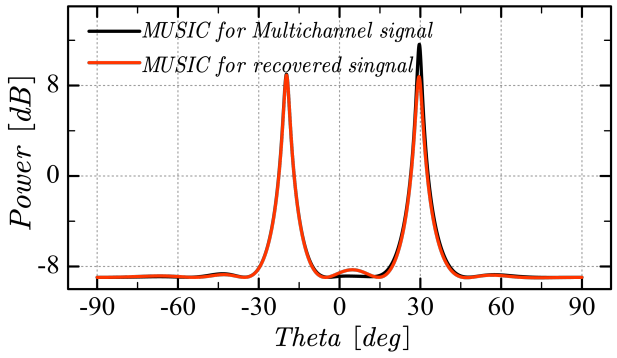

Fig. 5. Spatial spectral for uncorrelated source.

Second, Fig. 5 displays the spatial spectrum of the original QPSK signal with an incident direction of $(-20°, 30°)$ and the time-modulated received signal using the MUSIC algorithm. The figure reveals that the multi-channel received matrix recovered using a single-channel time-modulated super-surface can obtain a high-resolution spatial spectrum. Therefore, the proposed scheme can obtain multi-channel signals using a single-channel receiving array, which proves the effectiveness of the proposed scheme.

Finally, based on the analysis in Section II, an equivalent multi-dimensional receiving matrix is obtained by separating

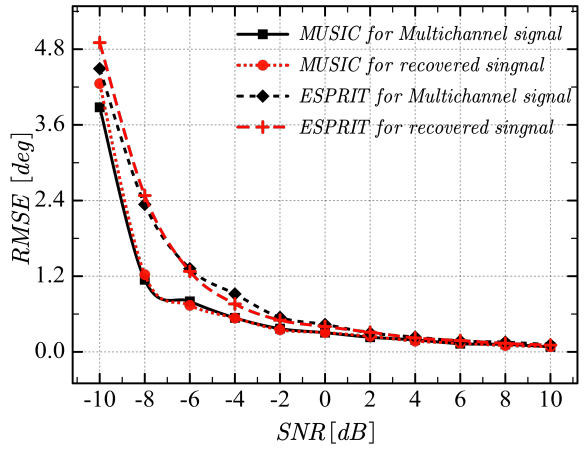

Fig. 6. RMSEs of DOA estimation versus SNR.

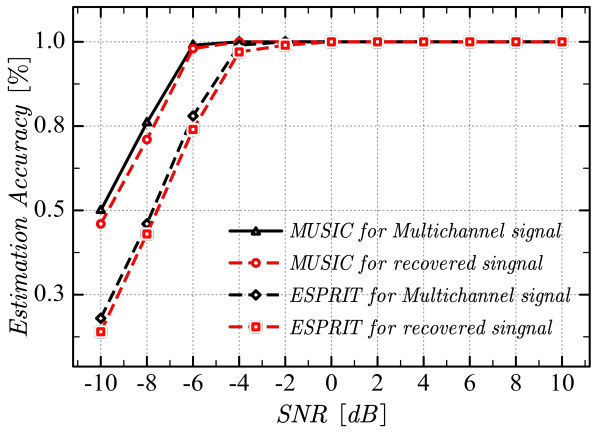

Fig. 8. Estimation resolution versus SNR.

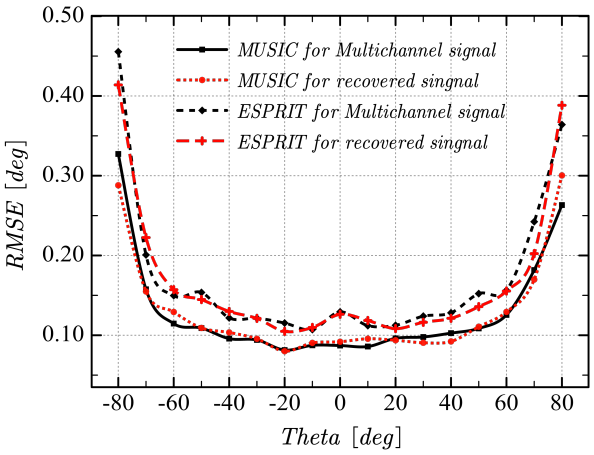

Fig. 7. RMSEs of DOA estimation versus incident directions.

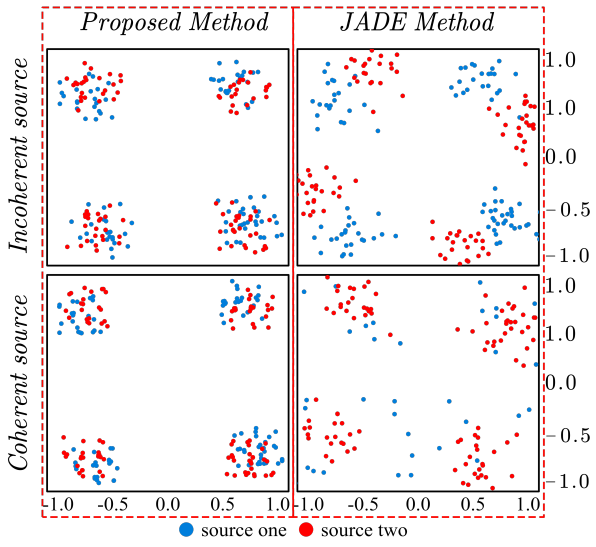

Fig. 9. Constellation diagram after signal separation.

different frequency signals through a filter. Subsequently, a multi-channel receiving matrix is obtained. In this section, two classical DOA estimation algorithms are used to process the standard multi-channel receiving matrix and the receiving matrix obtained from the proposed scheme to evaluate the performance of the proposed scheme.

Consider that SNR increases from -10 dB to 10 dB in steps of 2 dB. The variation of RMSEs under different SNR are depicted in Fig. 6, when incident direction is $(-20°, 30°)$. Assume that incident direction changing from $-90°$ to $90°$ with a step of $10°$. The variation of RMSEs under different incident direction is depicted in Fig. 7, when $SNR = 0$ dB. Fig. 9 displays the variation of estimation resolution with the SNR ratio using MUSIC and ESPRIT algorithms when the incident direction is $(-20°, 30°)$. The processed multi-channel receiving matrix in the two algorithms can accurately approximate the estimation ability of the original signal, which proves the proposed scheme can achieve the DOA estimation for multi-channel signals.

B. Signal Separation Performance

In this section, we consider two co-channel signals with an incoming direction of $(-30°, 20°)$. First, we used the MUSIC algorithm for DOA estimation and used the results as a basis for signal separation. We evaluate the performance of signal separation from the received signal constellation diagram, the received signal demodulation error rate, and the SINR of the received signal. In addition, we provide experimental results using the JADE algorithm for multi-channel received signals to compare the performance of signal separation.

First, Fig. 9 displays the constellation diagram after signal separation using the proposed and JADE algorithm at a SNR of 10 dB. Both the proposed and JADE algorithm can separate co-channel signals from different directions of arrival. However, the proposed algorithm achieves superior separation performance and a concentrated constellation diagram. Although the JADE algorithm cannot separate signals when separating coherent signal sources, the proposed algorithm still

TABLE II
THE SIMILARITY COEFFICIENT MATRIX OF TWO ALGORITHMS.

Two QPSK signals	Proposed methed	JADE method
Incoherent signal	0.9927 0.0015 0.0119 0.9940	0.9990 0.1002 0.0735 0.9974
Coherent signal	0.9460 0.4155 0.3996 0.9523	0.6322 0.8180 0.7434 0.7519

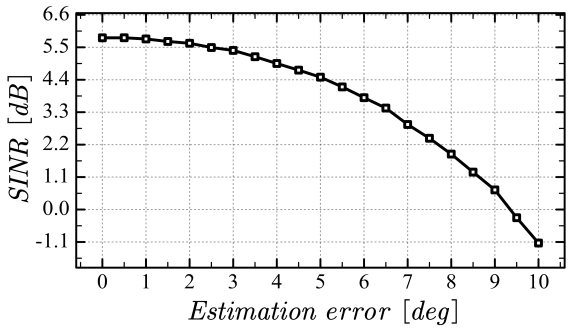

Fig. 10. SINR of signal separation versus estimation error.

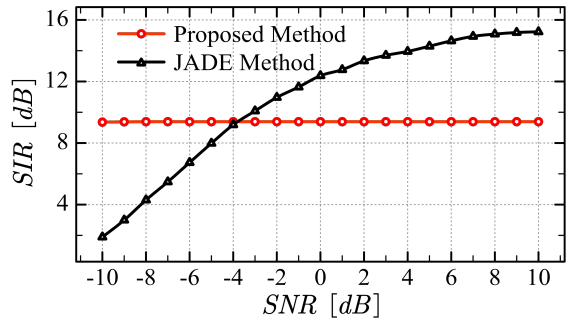

Fig. 11. SIR of signal separation versus SINR.

exhibits decent performance. To verify the signal separation effect of the proposed algorithm, Table II presents the similarity coefficients between the separated and source signals. Both algorithms can separate well for noncoherent signals. However, the proposed algorithm can filter out other. In the case of coherent signals, the proposed algorithm exhibits a certain separation ability, but some interference signals remain.

Because the proposed signal separation scheme used spatial filtering, its performance was only affected by the DOA estimation error when the array aperture was the same. Therefore, Fig. 10 displays the variation of the received signal SINR with DOA estimation error for noncoherent signal separation using the proposed algorithm when the SNR is 0 dB. The signal separation effect decreases with the increase in the DOA estimation error. However, when the DOA estimation error is within 3°, the SINR improvement ability will not decrease considerably. The proposed DOA estimation scheme can be maintained within 3 degrees. Therefore, this scheme is less affected by the SNR and is robust.

To verify the robustness of this scheme, Fig. 11 displays the variation of the signal-to-interference-plus-noise ratio (SIR) with SNR using the proposed algorithm and JADE algorithm for noncoherent signal separation. SIR can measure the difference in power between the two signals after separation, and the larger the SIR, the better the separation effect. The figure reveals that both schemes can improve the received signal SIR, for conventional signal separation schemes is affected by signal-to-noise ratio, SIR performs better at a high SNR. However, the improvement effect of the scheme of proposed is independent of the SNR, which is because the signal separation effect in this proposal comes from the gain difference of weighted directional patterns for different arrival directions. The effect of this scheme is mainly affected by the accuracy of DOA estimation and less affected by the SNR, and the upper limit of improvement is limited by the array aperture.

V. CONCLUSION

In this study, we proposed and subsequently validated a simple and cost-effective single-channel DOA estimation and signal separation algorithm based on the grouping scheme of TVM. In the proposed algorithm, TVM is grouped to generate various harmonic signals on different sub-surfaces and use different frequency harmonics to obtain the conventional multi-channel received signal matrix for DOA estimation. Based on the DOA estimation, the weighted directional diagram is used to separate the signals from different directions of arrival. Numerical simulations verify the performance of DOA estimation and signal separation. The proposed scheme can achieve excellent DOA estimation in a single channel to ensure the probability of accurate estimation and excellent separation performance of the signal separation scheme with strong robustness.

REFERENCES

[1] Z. Wei, F. Liu, C. Masouros, N. Su, and A. P. Petropulu, "Toward multi-functional 6G wireless networks: Integrating sensing, communication, and security," *IEEE Commun. Mag.*, vol. 60, no. 4, pp. 65–71, 2022.
[2] A. Chaoub *et al.*, "6G for bridging the digital divide: Wireless connectivity to remote areas," *IEEE Wireless Commun.*, vol. 29, no. 1, pp. 160–168, 2021.
[3] H. Sarieddeen, N. Saeed, T. Y. Al-Naffouri, and M.-S. Alouini, "Next generation terahertz communications: A rendezvous of sensing, imaging, and localization," *IEEE Commun. Mag.*, vol. 58, no. 5, pp. 69–75, 2020.
[4] Z. Zhang *et al.*, "A general channel model for integrated sensing and communication scenarios," *IEEE Commun. Mag.*, vol. 61, no. 5, pp. 68–74, 2022.
[5] K. Xu *et al.*, "Channel feature projection clustering based joint channel and DoA estimation for ISAC massive MIMO OFDM system," *IEEE Trans. Veh. Technol.*, vol. 73, no. 3, pp. 3678–3689, 2024.
[6] R. Schmidt, "Multiple emitter location and signal parameter estimation," *IEEE Trans. Antennas Propag.*, vol. 34, no. 3, pp. 276–280, 1986.
[7] R. Roy, A. Paulraj, and T. Kailath, "Direction-of-arrival estimation by subspace rotation methods - ESPRIT," in *Proc. IEEE ICASSP*, 1986.
[8] J. Tropp, "Greed is good: Algorithmic results for sparse approximation," *IEEE Trans. Inf. Theory*, vol. 50, no. 10, pp. 2231–2242, 2004.
[9] F. Liu, C. Masouros, A. P. Petropulu, H. Griffiths, and L. Hanzo, "Joint radar and communication design: Applications, state-of-the-art, and the road ahead," *IEEE Trans. Commun.*, vol. 68, no. 6, pp. 3834–3862, 2020.

[10] C. Jutten and J. Herault, "Blind separation of sources, part I: An adaptive algorithm based on neuromimetic architecture," *Signal Process.*, vol. 24, no. 1, pp. 1–10, 1991.
[11] A. Hyvarinen, "Fast and robust fixed-point algorithms for independent component analysis," *IEEE trans. Neural Netw.*, vol. 10, no. 3, pp. 626–634, 1999.
[12] J.-F. Cardoso, "High-order contrasts for independent component analysis," *Neural Comput.*, vol. 11, no. 1, pp. 157–192, 1999.
[13] Z. Yuan, Z. Yang, and E. Oja, "Projective nonnegative matrix factorization: Sparseness, orthogonality, and clustering," *Neural Process. Lett.*, pp. 11–13, 2009.
[14] D. Lee and H. S. Seung, "Algorithms for non-negative matrix factorization," *Advances Neural Inf. process. Syst.*, vol. 13, 2000.
[15] F. Zardi, P. Nayeri, P. Rocca, and R. Haupt, "Artificial intelligence for adaptive and reconfigurable antenna arrays: A review," *IEEE Antennas Propag. Mag.*, vol. 63, no. 3, pp. 28–38, 2020.
[16] Z. Wan *et al.*, "Ris-assisted integration of communications and security: Protocol, prototyping, and field trials," *IEEE Internet Things J.*, vol. 11, no. 16, pp. 26877–26887, 2024.
[17] P. He, T. She, W. Li, and W. Yuan, "Single channel blind source separation on the instantaneous mixed signal of multiple dynamic sources," *Mechanical Syst. Signal process.*, vol. 113, pp. 22–35, 2018.
[18] Q. Wu and R. Zhang, "Towards smart and reconfigurable environment: Intelligent reflecting surface aided wireless network," *IEEE commun. Mag.*, vol. 58, no. 1, pp. 106–112, 2019.
[19] Z. Zhu *et al.*, "Active reconfigurable intelligent surface enhanced Internet of medical things," *IEEE J. Biomed. Health Inform.*, vol. 28, no. 7, pp. 3831–3840, 2023.
[20] Z. Zhu *et al.*, "Robust beamforming design for IRS-aided secure SWIPT terahertz systems with non-linear EH model," *IEEE Wireless Commun. Lett.*, vol. 11, no. 4, pp. 746–750, 2022.
[21] Z. Zhu *et al.*, "Secrecy rate optimization in nonlinear energy harvesting model-based mmwave IoT systems with SWIPT," *IEEE Syst. J.*, vol. 16, no. 4, pp. 5939–5949, 2022.
[22] J. Xu *et al.*, "Sum secrecy rate maximization for IRS-aided multi-cluster MIMO-NOMA terahertz systems," *IEEE Trans. Inf. Forensics Security*, vol. 18, pp. 4463–4474, 2023.
[23] Z. Zhu *et al.*, "Intelligent reflecting surface-assisted wireless powered heterogeneous networks," *IEEE Trans. Wireless Commun.*, vol. 22, no. 12, pp. 9881–9892, 2023.
[24] Z. Zhu *et al.*, "Resource allocation for intelligent reflecting surface assisted wireless powered IoT systems with power splitting," *IEEE Trans. Wireless Commun.*, vol. 21, no. 5, pp. 2987–2998, 2021.
[25] S. Hu, F. Rusek, and O. Edfors, "Beyond massive MIMO: The potential of data transmission with large intelligent surfaces," *IEEE Trans. Signal Process.*, vol. 66, no. 10, pp. 2746–2758, 2018.
[26] J. Y. Dai, J. Zhao, Q. Cheng, and T. J. Cui, "Independent control of harmonic amplitudes and phases via a time-domain digital coding metasurface," *Light: Science & Appl.*, vol. 7, no. 1, p. 90, 2018.
[27] Z. Wan *et al.*, "Physical-layer key generation based on multipath channel diversity using dynamic metasurface antennas," *China Commun.*, vol. 20, no. 4, pp. 153–166, 2023.
[28] J. Wei Wang *et al.*, "High-precision direction-of-arrival estimations using digital programmable metasurface," *Advanced Intell. Syst.*, vol. 4, no. 4, p. 2100164, 2022.
[29] S. Chen, B. Sima, F. Xi, W. Wu, and Z. Liu, "Super-resolution DoA estimation using dynamic metasurface antenna," in *Proc. IEEE EuCAP*, 2020.
[30] M. Lin *et al.*, "Single sensor to estimate DoA with programmable metasurface," *IEEE Internet Things J.*, vol. 8, no. 12, pp. 10187–10197, 2021.

Ming Chen received his B.E. degree in Information Engineering University, Zhengzhou, China, in 2024. His research interests include wireless communication security and direction-of-arrival estimation.

Liang Jin received the Ph.D. degree from Xi'an Jiaotong University. He is currently a Professor and Ph.D. Supervisor of the PLA Strategic Support Force Information Engineering University, Zhengzhou, China. His research interests include wireless communication, physical layer security, and smart antenna.

Zheng Wang received his Ph.D. degree in Information Engineering University, Zhengzhou, China, in 2024. He is now an Assistant Researcher at the PLA Academy of Military Science. His research interests include wireless communication security and smart reconfigurable environments.

Zheyuan Deng received the B.E. degree in Electronic and Telecommunication Engineering from Information Engineering University, Zhengzhou, China in 2022, where he is currently working toward the Ph.D. degree in Information Engineering. His research interests include reconfigurable intelligent surface and wireless communication security.

Bo Zhang Associate Professor at National University of Defense Technology, with a research focus on wireless information security

Yajun Chen received the B.E. degree from UESTC University, and the M.S. and Ph.D. degrees from Information Engineering University, Zhengzhou, China. He has been a Faculty Member of Information Engineering University, since 2017. His research interests include wireless communications and physical layer security.

Kaizhi Huang received her B.E. degree in Digital Communication and M.S. degree in Communication and Information system from Information Engineering University, and Ph.D. degrees in Communication and Information system from Tsinghua University, Beijing, China, in 1995, 1998, and 2003 respectively. She has been a Faculty Member of NDSC since 1998, where she is currently a Professor and Director of Laboratory of Mobile Communication Networks. Her research interests include wireless network security and signal processing.